

Formation of Magnonic Waveguides via Surface Anisotropy-Induced Bragg Mirrors

Grzegorz Centała^{1*} and Jarosław W. Klos¹

¹*Institute of Spintronics and Quantum Information,
Faculty of Physics and Astronomy, Adam Mickiewicz University, Poznań,
Poland, Uniwersytetu Poznańskiego 2, 61-614 Poznań, Poland.*

(Dated: January 3, 2025)

Waveguides are fundamental components for signal transmission in integrated wave-based processing systems. In this paper, we address the challenges associated with designing magnonic waveguides and propose a novel type with promising properties. Specifically, we study a magnonic waveguide formed within a uniform ferromagnetic layer ($\text{Co}_{20}\text{Fe}_{60}\text{B}_{20}$) through surface anisotropy applied in stripe regions, creating Bragg mirror structures. The proposed waveguide enables the propagation of high-frequency spin waves with high velocities in the ferromagnetic layer while avoiding static demagnetizing effects. Using finite element simulations, we calculate the dispersion relation of the waveguide modes and analyze their spatial profiles. Additionally, we evaluate the group velocity and localization characteristics, providing a comprehensive understanding of the waveguide's performance.

I. INTRODUCTION

Magnonics uses spin waves to process signals at gigahertz frequencies in nanometer-sized reconfigurable systems. These properties make magnonics attractive compared to other technologies used for wave-based computing[1, 2], such as photonics or phononics, where reconfigurability or nanoscale integration require more efforts [3–6].

In devices consisting of multiple functional blocks, information must be efficiently transmitted between them. In wave-processing devices, including magnonic systems [7], this function is realized by waveguides. Magnonic waveguides can be implemented in many different ways. Some conventional techniques are shared with other technology platforms, such as photonics [8]. Others, however, are typical of magnonic systems [9].

Conventional magnonic waveguides are usually in the form of flat wires[10–14] – see Fig. 1(a). However, their transmission properties are determined not only by geometry and material selection but also by the configuration of magnetization. In the absence of magnetocrystalline anisotropy and the lack of external magnetic fields, the shape anisotropy forces static magnetization to be oriented along the waveguide axis. In this configuration, the group velocity of the spin wave is significantly reduced[11]. By applying the strong field, one can align the magnetization perpendicularly to the axis of the wire, which increases the group velocity, however, this simultaneity generates the wells of static demagnetization field near the edges of the waveguide and induces so-called edge modes[13, 14]. The partial solution to this problem is to use a waveguide in the form of a chain of dipolarly coupled nanoelements with shape anisotropy orienting magnetization perpendicular to the axis of the waveguide

without the necessity of application of external magnetic field[15].

Another technique to create a waveguide is the spatial modification of the material composition[16], which is also used to fabricate planar one-dimensional magnonic crystals[15, 17]. If the saturation magnetization M_s is lower in the waveguide region – see Fig. 1(b), then we can confine and guide the spin waves of frequencies lower than the ferromagnetic resonance (FMR) frequency of the layer in which the waveguide is embedded.

The most significant disadvantages of conventional waveguides, therefore, include: (i) limited reconfigurability - the geometry of the waveguide is fixed in the fabrication process, and changing its magnetic configuration must be done by applying a strong external magnetic field - which is technically difficult, (ii) the occurrence of strong static demagnetizing field (when the field is applied particularly the waveguide) or propagation speed limitation (when the field is applied along to the waveguide). It seems that a possible way to overcome these problems is to use a homogeneous layer as a conductor for spin waves with induced waveguide(s). Magnetic waveguides can be imprinted or spontaneously formed as magnetic domains[18–20] or domain walls[21, 22]. The temperature gradient[23], inhomogeneous Oersted field[24], inhomogeneous demagnetizing field[25]. One promising technique involves locally modifying the surface anisotropy to create magnonic waveguides within a uniform ferromagnetic layer – see Fig. 1(c). In such system, the spin waves of lower frequencies can be guided within trenches of the effective magnetic field landscape shaped by the modification of the surface anisotropy.[26]. This approach was also used to design various magnonic systems: magnonic crystals[27, 28], tunnel junctions[29], circulators[30].

However, these solutions where the waveguide is imprinted in a ferromagnetic layer [Fig.1(b,c)] allow for confinement and guidance of the spin waves only in a small range of frequencies limited up to the FMR frequency of

* grzcen@amu.edu.pl

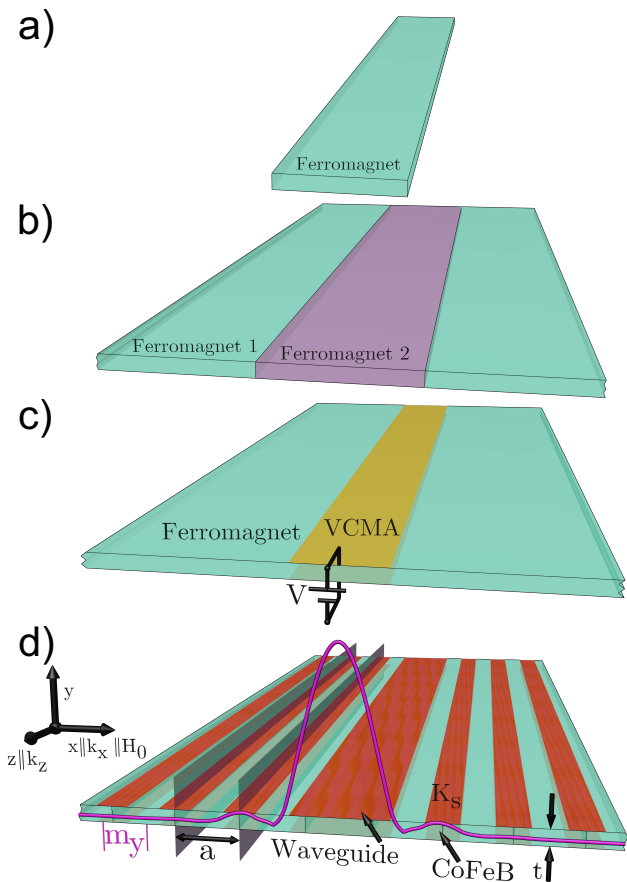


FIG. 1. Selected designs of planar magnonic waveguides: (a) Geometric confinement: a strip of ferromagnetic material. (b) Material parameter modification: a waveguide formed in the central region with reduced saturation magnetization. (c) Voltage-controlled surface anisotropy (VCMA): a waveguide induced by surface anisotropy. (d) Anisotropy-induced Bragg mirrors: a waveguide formed by surface anisotropy applied periodically at the top and bottom surfaces (red areas). The surface anisotropy strength is defined by the surface anisotropy constant K_s ; the period of the Bragg mirrors is denoted by a . The static magnetic field H_0 is applied in the plane, perpendicularly to the waveguide. The magenta line shows the exemplary spin wave profile (out-of-plane component $|m_y|$) confined in the waveguide.

pristine layer. Also, the strength of this confinement, i.e. the rate of exponential decay of the spin wave outside the waveguide, depends on the contrast of material parameters (saturation magnetization M_s or surface anisotropy constant K_s) and decreases to zero as the frequency approaches the upper limit of the mentioned range.

To overcome these limitations and realize the waveguide functionality for higher frequencies, we are going to consider a pair of semi-infinite 1D magnonic crystals (acting as Bragg mirrors[31]) to confine the spin waves in linear defect[32, 33] (1D cavity) – see Fig. 1(d). In the proposed system, spin waves can be confined in several frequency ranges, corresponding to the frequency gaps of the magnonic crystals. In our approach, the magnonic

crystals will be created by applying surface anisotropy while preserving the uniformity of the magnetic layer [27]. It is worth noting that a similar approach has been used to produce magnonic crystals by applying non-magnetic metal elements to the ferromagnetic layer [34, 35].

We will show that by appropriately playing with the size of the structure, we can obtain both strong confinement of spin waves and a relatively high speed of their propagation along the waveguide.

The paper has the following structure. The results are preceded by a description of the structure under study and the computational methods employed in the work. The paper concludes with a summary of the findings.

II. STRUCTURE

We investigated the structure shown in Fig. 1(d). We considered a thin layer ($t=6$ nm) of ferromagnetic material ($\text{Co}_{20}\text{Fe}_{60}\text{B}_{20}$) characterized by low spin wave damping $\alpha = 0.0029$ [36]. Surface anisotropy was applied to the bottom and top of the layer by interfacing $\text{Co}_{20}\text{Fe}_{60}\text{B}_{20}$ with MgO. The periodically repeating regions of surface anisotropy (narrower red stripes in Fig. 1(d)) form the Bragg mirrors that confine the spin waves in the waveguide (wider red strip in the center of Fig. 1(d)). Such a structure can also be interpreted as a magnonic crystal of period $a = 100$ nm with a defect. The width of the narrower strips (in the magnonic crystal) is 50 nm, while the width of the wide strips (defect) is 150 nm. All gaps between strips with applied surface anisotropy are 50 nm wide. We assume that the volume magnetocrystalline anisotropy can be neglected in our studies.

In our calculations, we used experimentally obtained values for the magnetization saturation $M_s = 1150$ kA/m [37], the exchange stiffness constant $A = 28$ pJ/m [36], and the gyromagnetic ratio $|\gamma| = 176$ rad/T/ns [36]. We used the experimentally determined surface anisotropy constant for MgO/CoFeB interfaces with Ta capping [37]. To enhance the role of the surface anisotropy we assumed that the surface anisotropy equally affects the top and bottom surfaces of the CoFeB layer ($K_s = 1.05$ mJ/m²). For comparison, we simulated the system within the surface anisotropy which is applied on only one surface, but with a doubled value of the surface anisotropy constant: $K_s = 2.1$ mJ/m² – see Supp. Note 1.

The external magnetic field used in the simulation ($\mu_0 H_0 = 500$ mT) is applied in the x -direction, perpendicular to the strips and tangential to the layer. In this geometry, spin waves propagate in the waveguide perpendicular to the applied field, ensuring the high group velocity characteristic of the Damon-Eshbach geometry. Notably, unlike the ferromagnetic strip [Fig. 1(a)], the proposed waveguide eliminates unwanted edge modes due to the absence of static demagnetization effects.

The localization within the considered waveguide results from the Bragg scattering of the spin waves, leading to the formation of magnonic gaps, which are crucial

for obtaining the waveguide modes of higher frequencies, i.e. higher than the FMR frequency of the pristine layer, which limits the operating frequencies of the waveguides shown in Fig. 1(b,c).

The chosen layer thickness $t = 6$ nm represents a compromise between two competing requirements: achieving a high spin-wave group velocity (which increases with t) [38] and maintaining a high effective anisotropy (which decreases with t) – see Supp. Note 2 for more details. The effective anisotropy is crucial for ensuring significant contrast in material parameters within the magnonic crystal, thereby enabling wide frequency gaps (that serve as the operating ranges for the waveguide) and strong spin wave confinement within the waveguide. The same reasoning, aimed at widening the frequency gaps, guided the choice of the magnonic crystal’s filling fraction (the ratio of the width of the surface anisotropy stripes to the period a) to be 50%. Additionally, a relatively small lattice constant ($a = 100$ nm) was selected to achieve a wide first Brillouin zone and to allow observation of a few lowest frequency bands at relatively high frequencies.

III. METHOD

In our study, we solved numerically the Landau-Lifshitz equation to describe the magnetization dynamics in the considered system:

$$\frac{d\mathbf{M}}{dt} = -\gamma\mu_0[\mathbf{M} \times \mathbf{H}_{\text{eff}} + \frac{\alpha}{M_s}\mathbf{M} \times (\mathbf{M} \times \mathbf{H}_{\text{eff}})] \quad (1)$$

where the symbol μ_0 denotes the vacuum permeability, α represents the damping constant, and $\mathbf{H}_{\text{eff}}(\mathbf{r}, t)$ is the effective magnetic field. We neglect the damping constant since it is small for considered material.

For the in-plane applied field the sample is magnetically saturated. As a result, we can easily linearize Eq. 1 by taking $\mathbf{M}(\mathbf{r}, t) = M_s\hat{\mathbf{x}} + \mathbf{m}(\mathbf{r})e^{i\omega t}$, where dynamic component oscillates harmonically in time[39].

The effective magnetic field $\mathbf{H}_{\text{eff}}(\mathbf{r}, t)$ consists of the external field of $H_0\hat{\mathbf{x}}$, the exchange field of $\mathbf{H}_{\text{ex}}(\mathbf{r}, t) = (2A/\mu_0M_s^2)\Delta\mathbf{M}(\mathbf{r}, t)$, and the dipolar field of $\mathbf{H}_{\text{d}}(\mathbf{r}, t) = -\nabla\varphi(\mathbf{r}, t)$. The magnetostatic potential is determined using the Gauss law for magnetism, under the magnetostatic approximation [40].

Uniaxial surface anisotropy is introduced by imposing boundary conditions. Since the dipolar pinning[41] do not play any role in our system, we can take the general for the boundary conditions for exchange-dominated spin waves: [17, 39] in the presence of uniaxial out-of-plane anisotropy.

$$\hat{\mathbf{x}} \times \frac{\partial \mathbf{m}}{\partial \hat{\mathbf{n}}} + \frac{K_s}{A} ((\hat{\mathbf{n}} \cdot \mathbf{m}) \hat{\mathbf{n}} \times \hat{\mathbf{x}} + (\hat{\mathbf{n}} \cdot \hat{\mathbf{x}}) \hat{\mathbf{n}} \times \mathbf{m}) = 0, \quad (2)$$

where $\hat{\mathbf{n}}$ is the unit vector normal to the surface.

The linearized form of Eq. 1, along with the Gauss equation for magnetism, was solved numerically using the

COMSOL Multiphysics environment, which employs the finite element method. The numerical computations were performed for a finite domain, with the following setups for different scenarios.

(i) Dispersion relation of infinite magnonic crystal: To calculate the dispersion relation and determine magnonic gaps, we considered a unit cell with Bloch boundary conditions: $\mathbf{m}(x)|_{x=a} = \mathbf{m}(x)|_{x=0} e^{ik_x a}$, where k_x , the x -component of the wave vector, was treated as a parameter. Simulations were conducted for the 2D domain of wave vector $\mathbf{k} = k_x\hat{\mathbf{x}} + k_z\hat{\mathbf{z}}$ plane to account for the non-isotropic the dispersion relation and determine properly the edges of the gaps for waveguide modes propagating in z -direction.

(ii) Waveguide modes localized in magnonic gaps: For the analysis of waveguide modes with frequencies within the magnonic gaps, a larger domain was used. Each magnonic crystal (Bragg mirror) was modeled with a length of 21 periods, and Bloch-Floquet boundary conditions were imposed at the ends of the structure. This large length allows the study of weakly localized waveguide modes.

Since the system is uniform in the z -direction, we assumed a plane wave solution of the form $\propto e^{ik_z z}$ in this direction, where k_z , the z -component of the wave vector, was treated as a model parameter.

Large non-magnetic regions are used above and below the layer, with a height about $1000t$, to correctly include the effect of the dynamic demagnetizing field outside the ferromagnetic layer on the magnetization dynamics.

IV. RESULTS

Due to shape anisotropy, the ferromagnetic resonance (FMR) frequency in a ferromagnetic layer is non-zero. Above the FMR frequency, the wave vector takes on real values, allowing spin waves to propagate through the layer. Conversely, below the FMR frequency, the wave vector becomes complex, leading to an unphysical exponential variation of the spin wave amplitude in an unconstrained layer. This property can be exploited to construct a waveguide (see Fig. 1(b,c)). By tuning the material parameters in the waveguide region, spin-wave modes can be quantized inside the waveguide, exhibiting exponential decay in the surrounding layer for frequencies only up to the FMR frequency of the layer. This limitation is removed if we use the pair of magnonic crystals to confine the spin waves in the waveguides, playing the role of the Bragg mirrors. The considered system (see Fig. 1(d)) overcomes such limitation and maintains the functionality of the waveguide for higher frequencies, from the frequency gaps where the complex wave vector ensures the confinement of the spin waves in the waveguide.

This feature is clearly visible in Fig. 2, where we can find the waveguide modes (blue lines) in many frequency gaps (white regions), including these laying high above

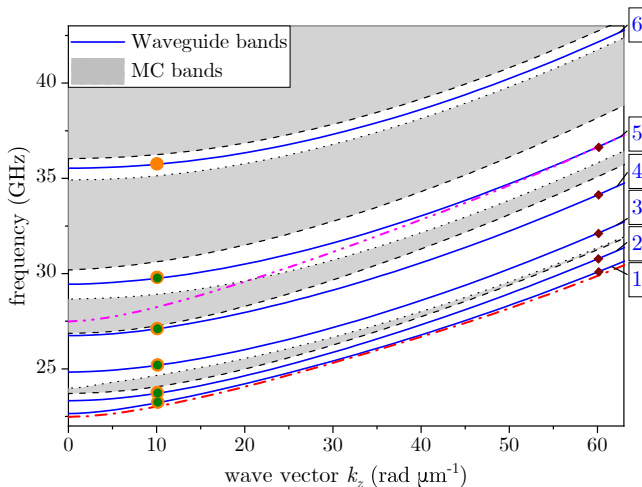


FIG. 2. Dispersion relation $f(k_z)$ of the waveguide modes for the structure shown in Fig. 1(d) (blue lines). The modes are confined within the waveguide when their frequencies lie within the frequency gaps of the magnonic crystals (white regions). The lowest possible frequency for the waveguide modes corresponds to the FMR frequency of a uniform layer with surface anisotropy applied on both sides (dot-dash red line). For the considered waveguide design, high-frequency waveguide modes (e.g., modes No. 5–6) can exist even above the FMR frequency of a uniform layer without surface anisotropy (dot-dot-dash magenta line). Olive circles and purple diamonds indicate the frequencies, f , and wave vectors, k_z , for which mode profiles were calculated (see Fig. 5). Orange circles mark the points where the figure of merit, quantifying the trade-off between propagation velocity and localization strength (see Supp. Note 2), was determined.

the FMR frequency of the uniform layer (dot-dot-dash magenta line).

In the considered frequency range, we can see one or two waveguide modes in successive frequency gaps but the number of these modes can be larger if we consider a wider waveguide. The number of waveguide modes in the selected gap depends also on the width of the gap, which, in turn, is related to the parameters of magnonic crystals.

We have shown that in the system under consideration the waveguide modes can be found, i.e. the modes propagating along the waveguide with the real wave number k_z and decaying when penetrating the Bragg mirrors at the exponential rate given by the imaginary part of the wave vector k_x from the frequency gap of the Bragg mirrors. However, this demonstration does not provide deep insight into the advantages of this design.

The large group velocity and strong location are the essential features of the waveguide that are decisive for its quality. Only significant value of the group velocity allows transmitting spin wave signal on the satisfactory distances in the presence of damping. On the other hand, the strong localization inside the waveguide reduces the cross-talks between different waveguides in the system.

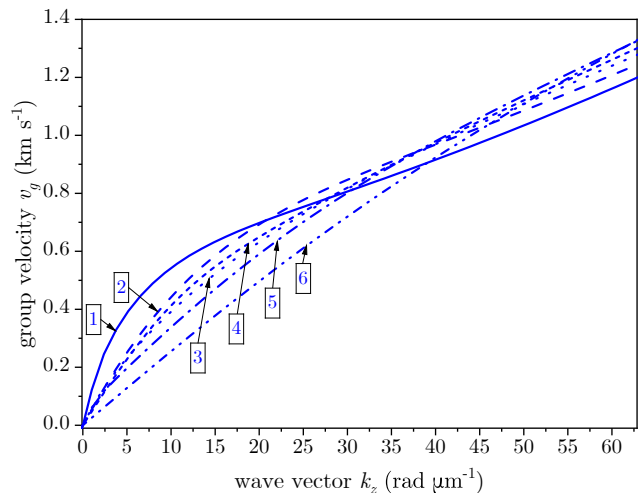


FIG. 3. Group velocity of the waveguide mode as a function of the wave vector, $v_g(k_z)$. The labels 1–6 correspond to successive modes of increasing frequencies (see Fig. 2) and increasing numbers of nodes within the waveguide (see Fig. 5).

Fig. 3 shows the group velocity of the waveguide modes, $v_g = d\omega/dk_z$, calculated from the dispersion relation. The group velocity of all modes increases with the wave vector k_z . For smaller values of k_z , the waveguide modes with the lowest frequencies exhibit higher group velocities; however, for larger k_z , this order is reversed. The obtained values of group velocities are suitable for spin wave transmission in low-damping materials such as CoFeB. However, the transmission of spin waves of long wavelengths is not effective v_g goes to zero for $k_z \rightarrow 0$.

The localization of waveguide modes is primarily determined by the complex wave vector, k_x , within the frequency gaps of the magnonic crystals. It is well established [42] that the imaginary part of the wave vector reaches its maximum within the frequency gap, indicating the strongest localization, and decreases toward the band edges. However, we used a general measure of localization: the Inverse Participation Ratio (IPR), which can be calculated from the profile of waveguide modes, $|m_y|$, across the entire structure. We computed a discrete approximation of the IPR: [43]

$$\widetilde{\text{IPR}} = \text{IPR} \frac{S}{mn} = \frac{\sum_{i,j}^{m,n} |m_y(x_i, y_j)|^4}{\left(\sum_{i,j}^{m,n} |m_y(x_i, y_j)|^2\right)^2}, \quad (3)$$

where $S = 43at$ is the cross-section area of the ferromagnetic layer. The number of points in the y -direction (across the thickness) is $n = 36$, while the number of points in the x -direction, (along the layer) is $m = 4300$. The $\widetilde{\text{IPR}}$ varies from $1/(mn)$ for the case of uniform distribution to a value of 1 for complete localization at one point only.

Fig. 3 shows the dependence of $\widetilde{\text{IPR}}$ on the wave vector k_z for successive waveguide modes. Note that the $\widetilde{\text{IPR}}$

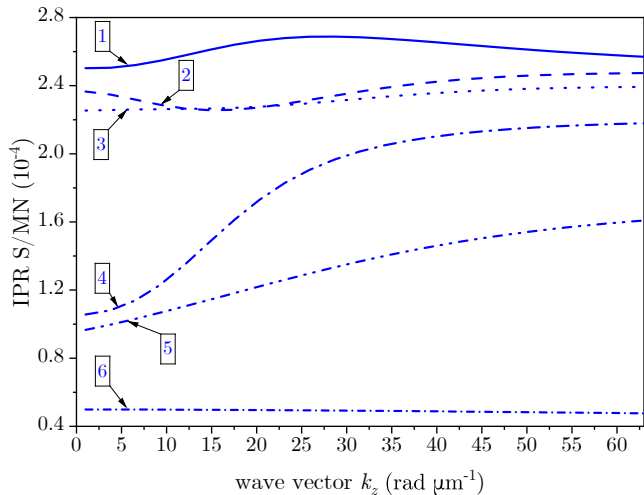


FIG. 4. The measure of the localization of the waveguide modes: modified Inverse Participation Ratio, $\widetilde{\text{IPR}}$, as a function of the wave vector, $\widetilde{\text{IPR}}(k_z)$. The localization is stronger for modes 1-3 of the frequencies below the FMR frequency of the uniform layer. The $\widetilde{\text{IPR}}$ is increasing with the wave number k_z when the mode's frequency is pushed toward the center of the frequency gap or the gap becomes wider – see modes No. 4 and No. 5 in Fig. 2.

values are largest for modes 1–3, which is clearly reflected in the mode profiles shown in Fig. 5. These modes have frequencies below the FMR frequency of the pristine ferromagnetic layer. This implies that the spin wave must tunnel (rather than oscillate in space) in the regions of the Bragg mirror where surface anisotropy has not been applied, explaining the faster spatial decay rate inside the whole Bragg mirrors: $\pm e^{\mp \Im(k_x)x}$. This faster decay rate corresponds to wider frequency gaps, where $\Im(k_x)$ reaches larger values.

Waveguide modes of higher frequencies (e.g., modes No. 4–6) can only be localized using Bragg mirrors. For some modes, such as No. 4 and No. 5, the localization strength changes noticeably with the wave vector k_z . This can be analyzed by examining the frequency changes of these modes with k_z in Fig. 2. As k_z increases, mode No. 4 moves away from the gap edge, while mode No. 5 moves closer to the gap edge. It is known[42] that both factors—proximity of the frequency to the center of the gap and increased gap width—enhance the localization strength of defect modes in periodic structures, as determined by the imaginary component of the wave vector ($\Im(k_x)$). The changes in localization strength with k_z are clearly visible in the profiles of modes No. 4 and No. 5—see Fig. 5, with the green and purple lines corresponding to different k_z values.

It is worth noting that the values of $\widetilde{\text{IPR}}$ and v_g are not independent of each other. The values of v_g can be increased by increasing the thickness t of the ferromagnetic layer[38]. However, the larger thickness will decrease the effective anisotropy $K_{\text{eff}} = -\mu_0 M_s^2 + K_s/t$ and make its

spatial alternation weaker, reducing the magnonic crystal (Bragg mirror) formation effect. Therefore, the reduction of K_{eff} would lead to the narrowing of the frequency gaps and the reduction of the localization strength expressed by $\widetilde{\text{IPR}}$. We discussed in Supp. Note 2 the section of the optimal layer thickness and the interplay between v_g and the $\widetilde{\text{IPR}}$.

The waveguide under consideration is a multimode waveguide. This means that, for a fixed frequency, many modes can be observed within the waveguide, each differing in the number of nodes. The number of accessible modes in multimode waveguide increases with frequency – see Fig. 2. To compare the entire set of possible modes, their profiles are plotted in Fig. 5 for fixed values of the wave vector k_z . Examining these profiles, two distinct regions can be identified: the waveguide region (the wider gray strip in the center), where the oscillation amplitude is relatively steady, and the Bragg mirror regions (magnonic crystals), where the oscillation amplitude decays exponentially. It is evident that the number of nodes in the waveguide region increases (from 0 to 4) for successive modes (Nos. 1–5) as the frequency rises, regardless of whether they appear individually or in pairs within the frequency gaps – see Fig. 2.

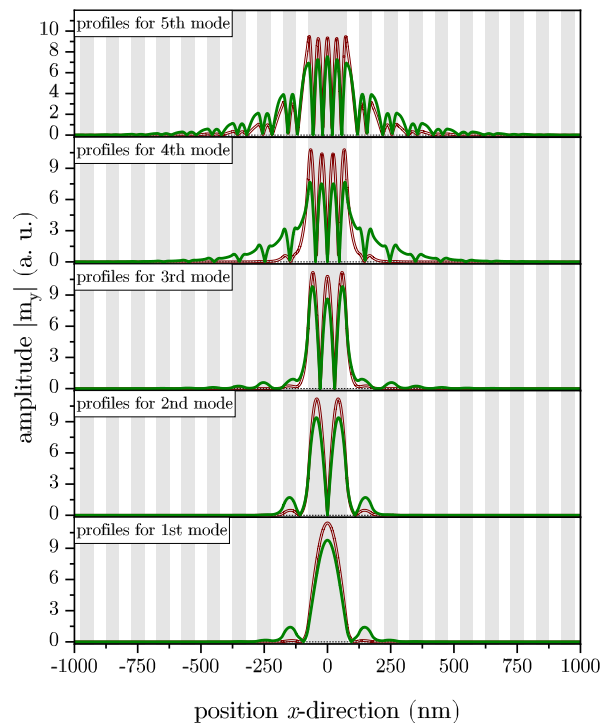


FIG. 5. Profiles of the out-of-plane component of the dynamic magnetization, $|m_y|$, for successive waveguide modes at two selected wave vector values: $k_z = 10 \text{ rad}/\mu\text{m}$ (green lines) and $k_z = 40 \text{ rad}/\mu\text{m}$ (purple lines). Refer to Fig. 2. The gray (white) regions mark the section of the layer with (without) surface anisotropy.

V. CONCLUSIONS

The suggested design exhibits notable advantages. Firstly, it relies upon a uniformly distributed magnetic layer characterized by low-damping ferromagnet, necessitating solely the imposition of a periodic pattern of non-magnetic material. Secondly, it effectively addresses the problem of the static demagnetizing field and obviates the occurrence of edge modes within the waveguide. Thirdly, the utilization of magnonic crystals featuring Bragg mirrors facilitates the propagation of higher mode frequencies along the waveguide when juxtaposed with analogous structures lacking Bragg mirrors.

Nevertheless, an inherent limitation of the proposed design lies in the requisite trade-off between achieving a high group velocity and fostering a robust magnonic crystal formation effect. This compromise mandates the incorporation of relatively high surface anisotropy constant values and necessitates the utilization of thin layers.

Considering all factors, we posit that the construction of such a system is relatively straightforward and lends itself to applicability in magnonic devices.

ACKNOWLEDGMENTS

This work has received funding from National Science Centre Poland grants UMO-2020/39/O/ST5/02110, UMO-2021/43/I/ST3/00550 and support from the Polish National Agency for Academic Exchange grant BPN/PRE/2022/1/00014/U/00001.

DATA AVAILABILITY

The data for the essential figures (Fig. 2, Fig. 3, Fig. 4) can be accessed via the following URL. The remaining data is available from the corresponding author on reasonable request.

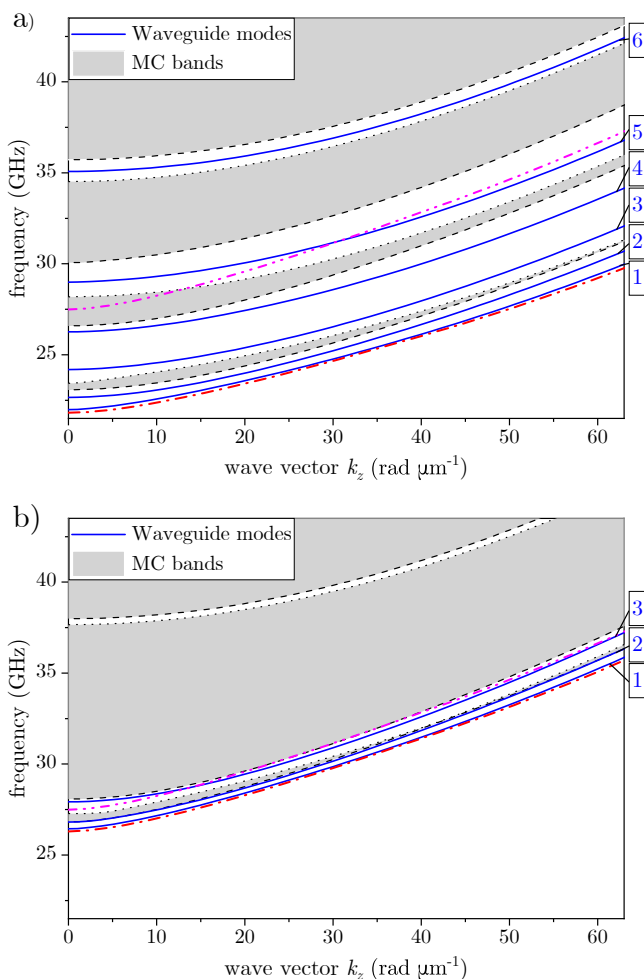
-
- [1] A. V. Chumak and et al., *IEEE Trans. Magn.* **58**, 1 (2022).
 - [2] A. Mahmoud, F. Ciubotaru, F. Vanderveken, A. V. Chumak, S. Hamdioui, C. Adelman, and S. Cotofana, *J. Appl. Phys.* **128**, 161101 (2020).
 - [3] W. Bogaerts, D. Pérez, J. Capmany, D. A. B. Miller, J. Poon, D. Englund, F. Morichetti, and A. Melloni, *Nature* **586**, 207 (2020).
 - [4] B. J. Eggleton, C. G. Poulton, P. T. Rakich, M. J. Steel, and G. Bahl, *Nat. Photonics* **13**, 664 (2019).
 - [5] S. R. Sklan, *AIP Adv.* **5**, 053302 (2015).
 - [6] J. C. Taylor, E. Chatterjee, W. F. Kindel, D. Soh, and M. Eichenfield, *npj Quantum Inf.* **8**, 1 (2022).
 - [7] A. Khitun and K. L. Wang, *Superlattice. Microst.* **38**, 184 (2005).
 - [8] R. A. S. D. Koala, M. Fujita, and T. Nagatsuma, *Nanophotonics* **11**, 1741 (2022).
 - [9] L. Zheng, L. Jin, T. Wen, Y. Liao, X. Tang, H. Zhang, and Z. Zhong, *J. Phys. D: Appl. Phys.* **55**, 263002 (2022).
 - [10] M. P. Kostylev, G. Gubbiotti, J.-G. Hu, G. Carlotti, T. Ono, and R. L. Stamps, *Phys. Rev. B* **76**, 054422 (2007).
 - [11] V. E. Demidov, S. O. Demokritov, K. Rott, P. Krzyteczko, and G. Reiss, *Phys. Rev. B* **77**, 064406 (2008).
 - [12] P. Pirro, T. Brächer, K. Vogt, B. Obry, H. Schultheiss, B. Leven, and B. Hillebrands, *phys. status solidi (b)* **248**, 2404 (2011).
 - [13] G. Duerr, K. Thurner, J. Topp, R. Huber, and D. Grundler, *Phys. Rev. Lett.* **108**, 227202 (2012).
 - [14] X. Xing, S. Li, X. Huang, and Z. Wang, *AIP Adv.* **3**, 032144 (2013).
 - [15] J. Ding and A. O. Adeyeye, *Adv. Funct. Mater.* **23**, 1684 (2013).
 - [16] B. Obry, P. Pirro, T. Brächer, A. V. Chumak, J. Osten, F. Ciubotaru, A. A. Serga, J. Fassbender, and B. Hillebrands, *Appl. Phys. Lett.* **102**, 202403 (2013).
 - [17] G. Centała, M. L. Sokolovskyy, C. S. Davies, M. Mruczkiewicz, S. Mamica, J. Rychły, J. W. Klos, V. V. Kruglyak, and M. Krawczyk, *Phys. Rev. B* **100**, 224428 (2019).
 - [18] E. Albisetti, D. Petti, M. Pancaldi, M. Madami, S. Tacchi, J. Curtis, W. P. King, A. Papp, G. Csaba, W. Porod, P. Vavassori, E. Riedo, and R. Bertacco, *Nat. Nanotechnol.* **11**, 545 (2016).
 - [19] S. J. Hämäläinen, M. Madami, H. Qin, G. Gubbiotti, and S. van Dijken, *Nat. Commun.* **9**, 4853 (2018).
 - [20] L. Wang, L. Gao, L. Jin, Y. Liao, T. Wen, X. Tang, H. Zhang, and Z. Zhong, *AIP Adv.* **8**, 055103 (2018).
 - [21] F. Garcia-Sanchez, P. Borys, R. Soucaille, J.-P. Adam, R. L. Stamps, and J.-V. Kim, *Phys. Rev. Lett.* **114**, 247206 (2015).
 - [22] K. Wagner, A. Kákay, K. Schultheiss, A. Henschke, T. Sebastian, and H. Schultheiss, *Nat. Nanotechnol.* **11**, 432 (2016).
 - [23] M. Vogel, A. V. Chumak, E. H. Waller, T. Langner, V. I. Vasyuchka, B. Hillebrands, and G. Von Freymann, *Nat. Phys.* **11**, 487 (2015).
 - [24] A. D. Karenowska, J. F. Gregg, V. S. Tiberkevich, A. N. Slavin, A. V. Chumak, A. A. Serga, and B. Hillebrands, *Phys. Rev. Lett.* **108**, 015505 (2012).
 - [25] M. Langer, F. Röder, R. A. Gallardo, T. Schneider, S. Stienen, C. Gatel, R. Hübner, L. Bischoff, K. Lenz, J. Lindner, P. Landeros, and J. Fassbender, *Phys. Rev. B* **95**, 184405 (2017).
 - [26] B. Rana and Y. Otani, *Phys. Rev. Appl.* **9**, 014033 (2018).
 - [27] S. Choudhury, A. K. Chaurasiya, A. K. Mondal, B. Rana, K. Miura, H. Takahashi, Y. Otani, and A. Barman, *Sci. Adv.* **6**, eaba5457 (2020).
 - [28] Q. Wang, A. V. Chumak, L. Jin, H. Zhang, B. Hillebrands, and Z. Zhong, *Phys. Rev. B* **95**, 134433 (2017).
 - [29] J. W. Klos, Y. S. Dadoenkova, J. Rychły, N. N. Dadoenkova, I. L. Lyubchanskii, and J. Barnaś, *Sci. Rep.*

- 8**, 17944 (2018).
- [30] J. Zhao, L. Feng, M. Ma, and F. Ma, *J. Magn. Magn. Mater.* **586**, 171161 (2023).
- [31] M. A. Morozova, A. V. Sadovnikov, O. V. Matveev, A. Y. Sharaevskaya, Y. P. Sharaevskii, and S. A. Nikitov, *J. Phys. D: Appl. Phys.* **53**, 395002 (2020).
- [32] R. A. Gallardo, T. Schneider, A. Roldán-Molina, M. Langer, A. S. Núñez, K. Lenz, J. Lindner, and P. Landeros, *Phys. Rev. B* **97**, 174404 (2018).
- [33] J. W. Klos and V. S. Tkachenko, *J. Appl. Phys.* **113**, 133907 (2013).
- [34] K. Mori, T. Koguchi, T. Watanabe, Y. Yoshihara, H. Miyashita, D. Grundler, M. Inoue, K. Ishiyama, and T. Goto, *Phys. Rev. Appl.* **21**, 014061 (2024).
- [35] M. Mruczkiewicz, M. Krawczyk, G. Gubbiotti, S. Tacchi, Y. A. Filimonov, D. V. Kalyabin, I. V. Lisenkov, and S. A. Nikitov, *New J. Phys.* **15**, 113023 (2013).
- [36] H. Wang, W. He, R. Yuan, Y. Wang, J. Wang, Y. Zhang, I. Medlej, J. Chen, G. Yu, X. Han, J.-P. Ansermet, and H. Yu, *Phys. Rev. B* **106**, 064410 (2022).
- [37] D.-S. Lee, H.-T. Chang, C.-W. Cheng, and G. Chern, *IEEE Trans. Magn.* **50**, 1 (2014).
- [38] D. Stancil and A. Prabhakar, *Spin Waves: Theory and Applications* (Springer US, 2009).
- [39] A. Gurevich and G. Melkov, *Magnetization Oscillations and Waves* (Taylor & Francis, 1996).
- [40] K. Szulc, S. Tacchi, A. Hierro-Rodríguez, J. Díaz, P. Gruszecki, P. Graczyk, C. Quirós, D. Markó, J. I. Martín, M. Vélez, D. S. Schmool, G. Carlotti, M. Krawczyk, and L. M. Álvarez Prado, *ACS Nano* **16**, 14168 (2022), pMID: 36043881.
- [41] K. Y. Guslienko, S. O. Demokritov, B. Hillebrands, and A. N. Slavin, *Phys. Rev. B* **66**, 132402 (2002).
- [42] W. Kohn, *Phys. Rev.* **115**, 809 (1959).
- [43] D. Thouless, *Phys. Rep.* **13**, 93 (1974).
- [44] X. Li, K. Fitzell, D. Wu, C. T. Karaba, A. Buditama, G. Yu, K. L. Wong, N. Altieri, C. Grezes, N. Kioussis, S. Tolbert, Z. Zhang, J. P. Chang, P. Khalili Amiri, and K. L. Wang, *Appl. Phys. Lett.* **110**, 052401 (2017).

SUPPLEMENTARY INFORMATION

SN 1. One-sided versus two-sided Bragg mirrors

The proposed model includes a Bragg mirror based on a large value of the surface anisotropy constant ($K_s = 1.05 \text{ mJ/m}^2$) applied periodically and equally to both the top and bottom surfaces of the ferromagnetic material. However, the equal contribution of surface anisotropy on both surfaces is not the usual case. Therefore, we have performed additional calculations in which we have implemented the twice as large surface anisotropy ($K_s = 2.1 \text{ mJ/m}^2$) only on the top surface. The resulting dispersion relation is shown in Supp. Fig. 1(a).



SUPP. FIG. 1. Dispersion relations for the waveguide with one-sided Bragg mirrors, i.e. when the surface anisotropy is applied only at the top of the ferromagnetic layer, a) $K_s = 2.1 \text{ mJ/m}^2$, b) $K_s = 0.54 \text{ mJ/m}^2$.

An alternative method of modifying the surface anisotropy is by applying an external electric field. The materials being considered (CoFeB/MgO) are

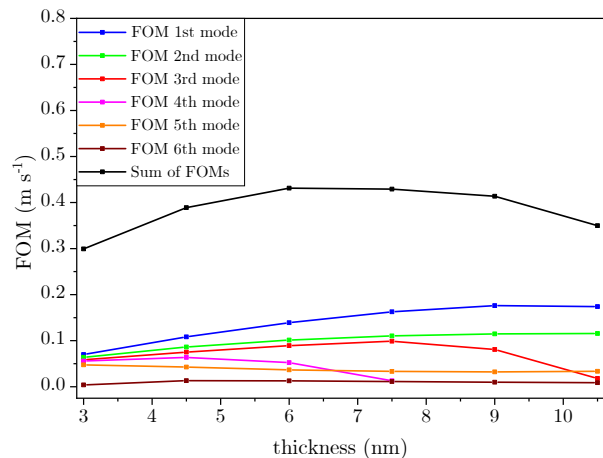
also suitable for voltage-controlled magnetic anisotropy (VCMA). With this method, we can achieve a value of $K_s = 0.54 \text{ mJ/m}^2$ [44].

We investigated the possibility of on-demand induction of a waveguide by applied voltage. Considering the same geometrical parameters, we use the value $K_s = 0.54 \text{ mJ/m}^2$ to form the Bragg mirrors only on the top surface. The dispersion relation obtained is presented in Supp. Fig. 1(b).

The number of frequency gaps decreased due to the almost four times smaller surface anisotropy constant. Consequently, the number of modes propagating in the waveguide decreased from six to three within the same frequency range.

SN 2. Selection of the layer thickness

The values of $\widetilde{\text{IPR}}$ and v_g are interconnected. Increasing the ferromagnetic layer thickness t can enhance v_g [38], but it reduces the effective anisotropy, $K_{\text{eff}} = -\mu_0 M^2 s + K_s/t$, weakening its spatial variations and diminishing the Bragg mirror effect. This results in narrower frequency gaps and reduced localization strength, as reflected by IPR.



SUPP. FIG. 2. Figure of merit (FOM) is presented as the product of the location measure ($\widetilde{\text{IPR}}$) and group velocity (v_g) of individual modes. Additionally, a black line represents the sum of FOMs for individual spin wave modes.

As a criterion for the selection of the layer thickness, we decided to use the following figure of merit $\text{FOM} = \widetilde{\text{IPR}} v_g$, where $\widetilde{\text{IPR}}$ is the reformulated inverse participation ratio, and v_g is the spin wave group velocity. The results obtained for $k_z = 10 \text{ rad}/\mu\text{m}$ are shown in Supp. Fig. 2. The resultant FOM, being a sum of FOM for all considered modes, contains local maximum for thicknesses 6 nm. This value can be easily identified with Supp. Fig. 2.

It is worth noting that for thicker layers, the 3rd and 4th

mods disappear. This is due to a shift in the dispersion relation with the thickness of the system. The shift in the dispersion relation results in the disappearance of mods propagating in the waveguide in areas accessible

to magnonic crystals. Conversely, it was not feasible to select a structure of lesser thickness due to the limitations imposed by the group velocity constraints.